



# Improvement of Vanadium Redox Flow Battery Efficiency Through Carbon Felt Electrodes Modification by Atmospheric Dielectric Barrier Discharge

Yuhan Li<sup>1</sup> · Juanjuan Lu<sup>1</sup> · Ming Gao<sup>2</sup> · Kangli Wang<sup>1</sup> · Zilan Xiong<sup>1</sup> · Kai Jiang<sup>1</sup>

Received: 15 May 2023 / Accepted: 24 July 2023 / Published online: 7 August 2023

© The Author(s), under exclusive licence to Springer Science+Business Media, LLC, part of Springer Nature 2023

## Abstract

Vanadium redox flow batteries (VRFBs) have become increasingly popular for energy storage, owing to their exceptional safety and scalability. However, the electrode material drawbacks still restrict the efficiency of the VRFBs. In this study, we employed atmospheric dielectric barrier discharge (DBD) to modify the commercial carbon felt (CF) electrodes for VRFB efficiency improvement. The treatment conditions were optimized by changing the gas composition and the treatment time. We found that the DBD modification could effectively enhance the coulombic efficiency (CE), voltage efficiency (VE), and energy efficiency (EE) of VRFB, and the improvements increased with the increase in N<sub>2</sub>:O<sub>2</sub> ratio and the treatment time. The most significant EE improvement was ~ 13.2% after 10 min DBD treatment. The electrolyte contact angle decreased with the treatment time and closely related to the battery efficiency. The X-ray photoelectron spectroscopy (XPS) results demonstrated that plasma treatment formed abundant hydrophilic functional groups, while the scanning electron microscope (SEM) results shown increased roughness on the CF surface. All the results indicated the DBD modification introduces hydrophilic groups onto the CF surface and increases the roughness, which could increase the reaction area and provide more active sites for the vanadium redox reaction hence enhance the VRFB efficiency.

**Keywords** Dielectric barrier discharge · All vanadium redox flow battery · Carbon felt · Material modification · Battery efficiency

---

✉ Zilan Xiong  
zilanxiong@hust.edu.cn

✉ Kai Jiang  
kjiang@hust.edu.cn

<sup>1</sup> State Key Laboratory of Advanced Electromagnetic Engineering and Technology, Huazhong University of Science and Technology, Wuhan 430074, China

<sup>2</sup> Shenzhen Institute of Advanced Technology, Chinese Academy of Sciences, Shenzhen 518055, China

## Introduction

VRFBs are developed to be one of the most commercially mature redox flow battery due to the characteristics of high energy efficiency, flexible design and low maintenance cost [1–3]. Electrode materials are critical component of VRFBs as they provide the sites for the redox reactions, even though they do not directly participate in the redox process as reactants [4]. CF has been widely used as the electrode material in VRFB systems, owing to its outstanding electrical conductivity, high stability, and cost advantage [5, 6]. However, the electrochemical performance of pristine CF electrode still needs improvement to further increase the efficiency of the VRFBs. Therefore, surface modification is necessary to enhance the reversibility in battery reactions, subsequently improving the energy efficiency and power density of VRFBs.

The common methods for CF modification include chemical reaction [7, 8], heat treatment [9, 10], microwave treatment [11] and plasma treatment [12–15]. Compared to other surface modification techniques, plasma modification presents several advantages, such as rapid processing, high energy density, and controllable gas conditions [16–19]. Huang et al. [13] used nitrogen and oxygen plasma (13.56 MHz RF source) to modify the CF electrode at low pressure and 200W. The modification improved the energy efficiency of VRFB from 65 to 78% with good cycling stability. However, general low-pressure plasma modification requires vacuum system and complex operational processes. Recently, atmospheric pressure plasma has been widely used for material modification due to its simplicity and high efficiency [20, 21]. Limited literatures have reported of CFs modification by using atmospheric pressure plasma for VRFBs efficiency improvement [22–24]. Lin et al. [23] used the nitrogen plasma jets to prepare a high performance CF electrode at atmospheric pressure, resulted in the energy efficiency of VRFB increased from 67.9% to 77.6%. Considering the large-scale uniform treatment and reduced the consumption of working gas, atmospheric dielectric barrier discharge (DBD) modification is more favorable than other plasma modification.

In this work, we employ atmospheric DBD to modify the commercial CF materials (with an initial EE as high as 76%) for VRFB efficiency improvement. By changing the composition of the working gas and treatment time, we systematically investigated the modification of CF on VRFB efficiency. We measured the VE, CE, and EE of the VRFB before and after CF modification, and optimized the modification parameters. Additionally, we employed XPS, SEM, and electrolyte/water contact angle measurements to explore the mechanisms behind the improvement of battery efficiency in VRFBs after DBD modification.

## Experimental Setup and Measurements

### Materials

Commercial CF (China, Haote new material company) was used as electrodes (3 cm×3 cm×0.4 cm in size) for electrochemical measurements in this work. Nafion membrane (China, Thinkre new material, N212, 54 μm) separated the positive and negative electrodes, facilitating ion exchange and redox reactions. The graphite sheets (China, Jinglong Carbon Company) were designed with a snake-shaped channel on the surface,

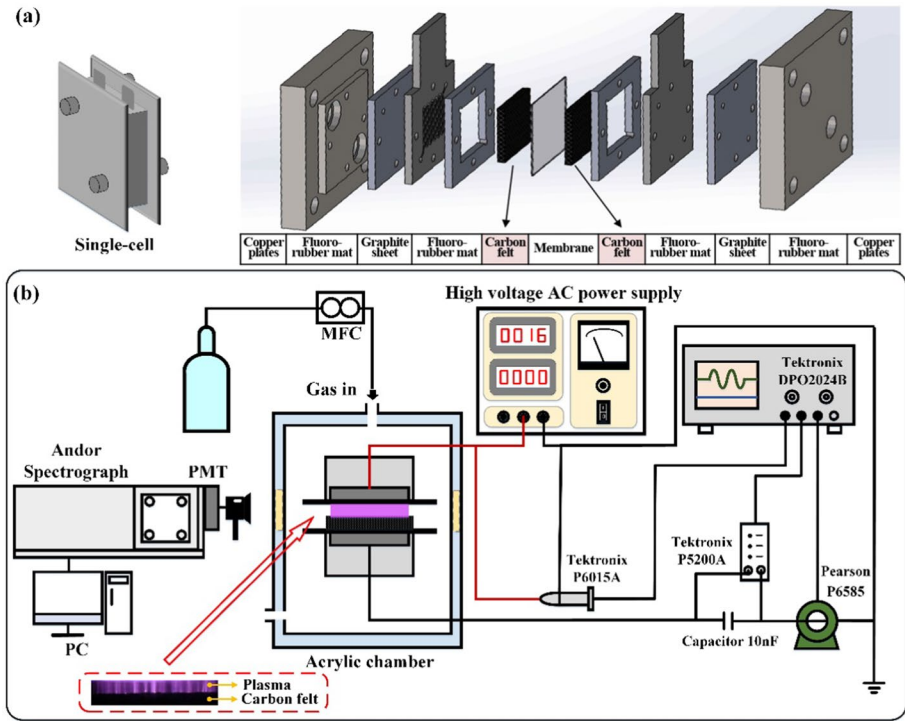


**Fig. 1** **a** Single-cell assembly used for VRFB efficiency tests. **b** Schematic diagram of experimental setup

which facilitates the flow of electrolytes. Figure 1a displays the assembly diagram and internal constitution of a single VRFB cell, which consists of a Nafion membrane, carbon felts, fluoro-rubber mats, graphite sheets, and copper plates.

### Experimental Setup

Figure 1b shows a schematic diagram of the experimental setup. Two copper electrodes (30 mm in diameter and 14 mm in high) wrapped in polytetrafluoroethylene (PTFE) were mounted inside an acrylic cylindrical chamber. Two SiO<sub>2</sub> dielectric plates with diameter of 80-mm and thickness of 1 mm were attached to the copper electrodes as dielectric. The CF was placed on the lower dielectric plate during treatment. The discharge gap (from the up side of the CF to the surface of the upper dielectric plate) was fixed at 2 mm. A high-voltage AC power was used to generate plasma in the discharge gap. The frequency of was fixed at 20 kHz. Two quartz windows (40 mm square) were mounted on the sidewall of the chamber for spectroscopic analysis.

In this study, N<sub>2</sub> and O<sub>2</sub> mixture were used as the working gases. To investigate the gas composition on the modification effect, four groups of working gases were employed, as shown in Table 1. The flow rate was regulated by flow meters, and for all the experiments, the total gas flow rate was fixed at 1L/min. For all the experiments, the chamber was purged with related working gas for 5 min to evacuate air before discharge.

**Table 1** Four groups of discharge gases used in this study

Types	N <sub>2</sub> (L/min)	O <sub>2</sub> (L/min)
N <sub>2</sub> (20%) + O <sub>2</sub> (80%)	0.2	0.8
N <sub>2</sub> (50%) + O <sub>2</sub> (50%)	0.5	0.5
N <sub>2</sub> (70%) + O <sub>2</sub> (30%)	0.7	0.3
N <sub>2</sub> (100%)	1	0

## Measurements and Methods

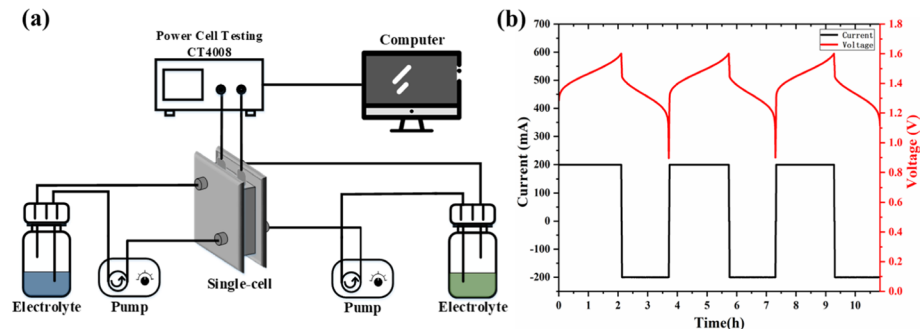
The discharge power was calculated using the Lissajous method [25], with a 10nF capacitor connected in series to the circuit. The voltage across the capacitor was measured using a differential probe (Tektronix, P5200A). The applied voltage and current were measured using a high-voltage probe (Tektronix, P6015A) and a current probe (Pearson, P6585), respectively. The optical emission spectrum (OES) was measured by using a spectrometer (AndorS, R-500I-A) equipped with a photomultiplier tube (Zolix, PMTH-S1).

The surface morphology of the CF was detected using a field scanning electron microscope (FSEM, FEI, Sirion200). X-ray photoelectron spectroscopy (XPS) measurements were conducted by AXIS-ULTRA (Kratos, DLD-600W) photoelectron spectrometer. The surface hydrophilicity was assessed by contact angle, using a water drop angle meter (SINDIN, SDC-500).

The single cell tests were conducted using a power cell tester (NEWARE, CT4008), as shown in Fig. 2a. The current density for constant current charge–discharge tests was set to 22 mA/cm<sup>2</sup>. The charge cut-off voltage was set to 1.6 V, and the discharge voltage was set to 0.9 V. The charge–discharge curves, as illustrated in Fig. 2b, were recorded to investigate the impact of CF modification on battery efficiency. The CE, VE, and EE were calculated using the following equations, respectively [24]:

$$VE = \frac{V_d}{V_c} \times 100\% \quad (1)$$

$$CE = \frac{Q_d}{Q_c} \times 100\% \quad (2)$$

**Fig. 2** a Schematic diagram of single cell test, b Charge–discharge curves of VRFBs

$$EE = VE \times CE \quad (3)$$

where  $V_d$  is the discharge midpoint voltage (V),  $V_c$  is the charging midpoint voltage (V),  $Q_d$  is discharge capacity (Ah),  $Q_c$  is the charging capacity (Ah).

## Results and Discussions

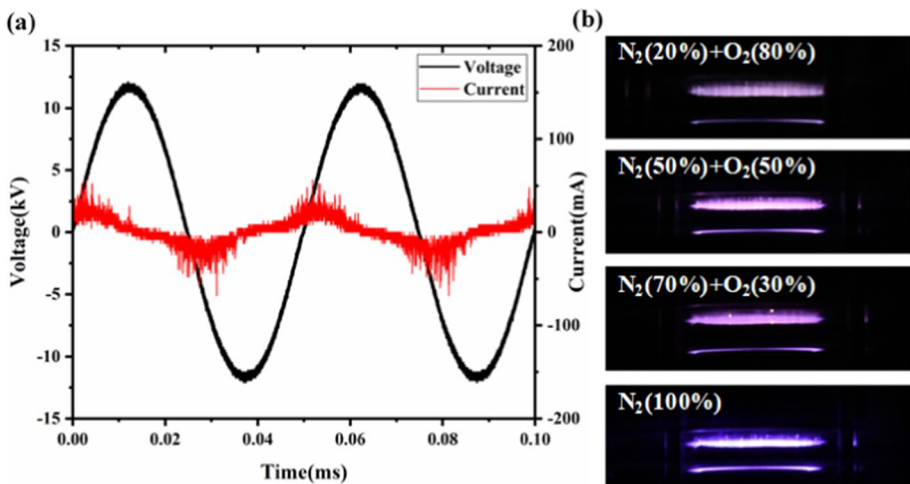
### Plasma Parameters

Figure 3a shows the typical voltage and current waveforms during treatment. The  $V_{p-p}$  of AC voltage was 25 kV and the frequency was fixed at 20 kHz. The discharge power for all the treatments the power was fixed at 25 W. Figure 3b presents the discharge images under various gas compositions. The intensity of the discharge increases with the reduction of  $O_2$  content as expected.

The OES results under different working gases are shown in Fig. 4. The major optical emission lines from atomic N, O, and the first positive band (FPS) and the second positive band (SPS) of  $N_2$  as well as  $N_2^+$  are observed [26, 27]. The spectral intensity becomes stronger as the proportion of  $N_2$  increases in the  $N_2/O_2$  mixture, which is consistent with the discharge intensity. In the  $N_2$  (100%) group, very weak emission of O at 777.2 nm was detected. The reason is that the whole chamber was not well sealed, and even we purged the gas inside the chamber for several minutes before treatment, the air could not be completely exhausted. Therefore, very little content of air still existed in the  $N_2$  (100%) group.

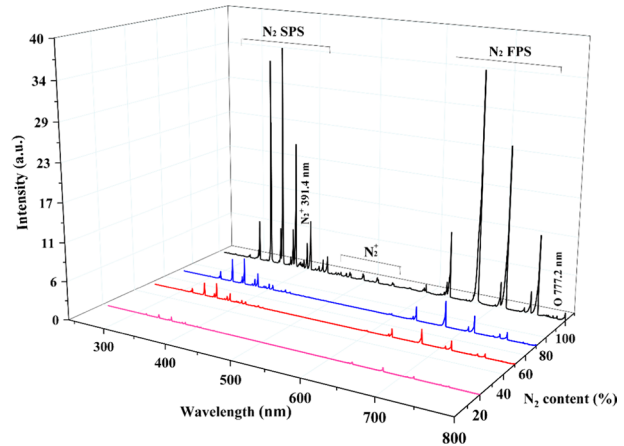
### The Modification Effect of Discharge Gas on VRFB Efficiency

Figure 5 shows the VE, CE, and EE of VRFB after CF modification with various discharge gas compositions. After a 5-min DBD treatment, the efficiency of each cell gradually

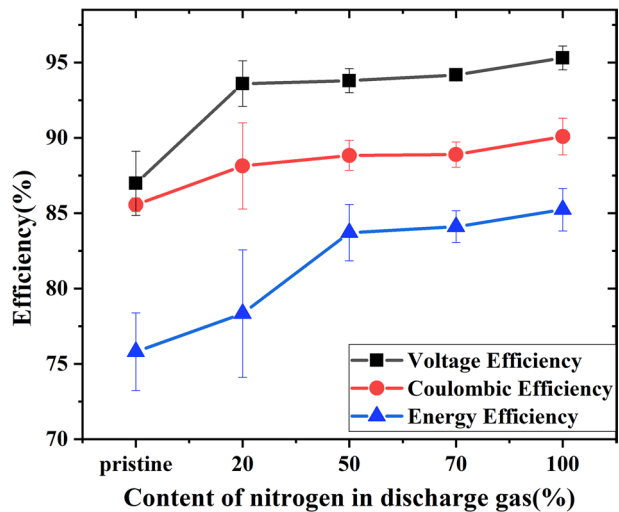


**Fig. 3** a Applied voltage and current waveforms; b Discharge images under various discharge gas

**Fig. 4** OES under various discharge gas



**Fig. 5** VE, CE and EE of VRFB with CF modification under various discharge gas



improves with increasing proportion of  $N_2$  in the discharge gas. Compared to the untreated CF, the battery exhibits improvements in VE from 87 to 96%, CE from 85 to 90%, and EE from 76 to 86%.

The observed enhancement in this experiment is close to that in other studies using non-commercial CF [13, 22]. However, the CFs used in those studies had a much lower EE before modification, which falls considerably short of the commercial market standards. In contrast, the CF utilized in this study already achieved an EE of 76% before modification, and a 13.2% improvement on this basis represents a significant enhancement.

### The Effect of Treatment Time on VRFB Efficiency

Based on the previous experiments, the modification result of  $N_2$  (100%) as the discharge gas has shown the most significant impact on improving VRFB efficiency. Therefore, we

**Fig. 6** Charge–discharge curves of VRFBs for various treatment time of N<sub>2</sub> DBD treatment

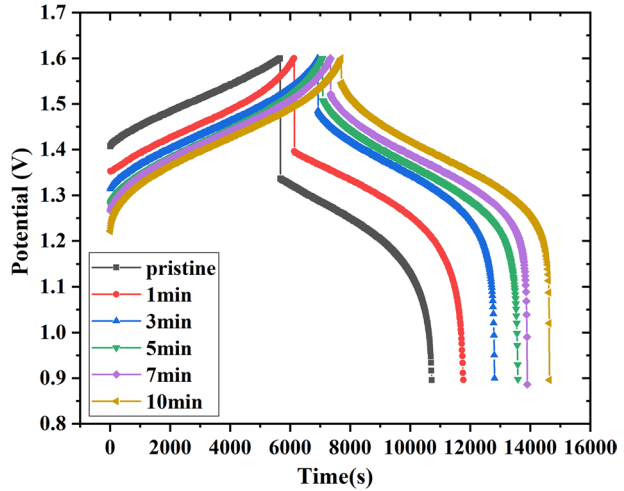
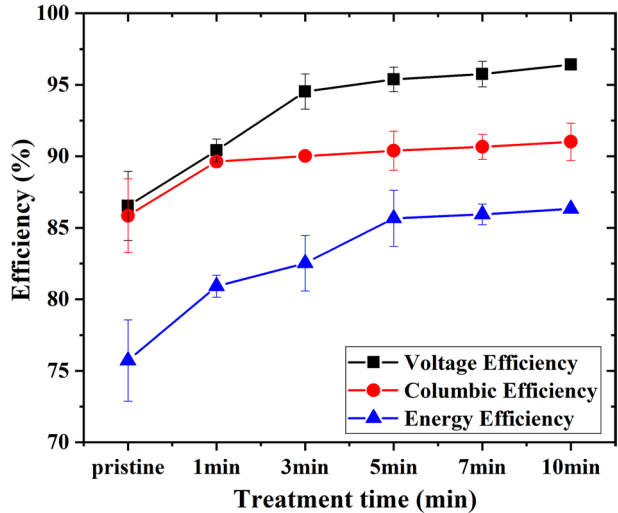


**Fig. 7** The change of VE, CE and EE vs. treatment time



further investigated the effect of the time gradient on VRFB efficiency. Figure 6 displays the voltage data of the first charge–discharge cycle of single cell treated with N<sub>2</sub> plasma. The charge–discharge curves reveal that with an increase in treatment time, the batteries shows a decrease in charge inception voltage and an increase in discharge inception voltage. Additionally, the cycle time of batteries become longer, which indicates that the VRFB has lower internal resistance and greater capacity after plasma modification.

Figure 7 illustrates the VE, CE, and EE of VRFB after N<sub>2</sub> plasma treatment vs. treatment time. All the efficiency of VRFB show an increasing trend with the increase of the treatment time. When up to 10 min, the VE increases from 86 to 97%, the CE increases from 85 to 91%, and the EE increases from 76 to 87%. Notably, after 7 min of treatment, the enhancement maintains at a satisfactory level and hardly to be further increased with the treatment time.

## The Properties of the CF Materials After Plasma Modification

In order to investigate the mechanism of the plasma modification of CFs on the enhancement of the VRFB efficiency, the material properties of the CFs before and after plasma treatment were detected and analyzed.

Figure 8 shows both the electrolyte and water contact angle results of the CFs vs. treatment time. The electrolyte contact angle and water contact angle on CF surface under the same condition are similar and both significantly decreases with the DBD modification time. The CF surface reaches complete hydrophilicity after 7 min and 10 min treatment, with a contact angle of  $0^\circ$ , as evidenced by the penetration of droplets into the CFs.

Interestingly, there is a growing trend in both hydrophilicity and the battery efficiency. With the extension of treatment time: the hydrophilicity and efficiency both significantly increased in the 1–5 min treated samples; and after 7–10 min treatment, when the CFs were completely hydrophilic, the VRFB efficiency hardly increased with further treatment. These results indicate that the DBD treatment can effectively enhance the VRFB efficiency through increasing the hydrophilicity of the CF surface.

XPS was employed to investigate the changes in surface chemical composition. The original and fitting results for the C1s and O1s components for pristine and CF treated with  $N_2$  plasma for 5 min are shown in Fig. 9 as an example. The data indicates that the content of C decreases after plasma treatment, the area of the C–C bond peak decreases, and the area of the oxygen-containing functional group peaks increases.

The atomic content change on the CF surface vs. treatment time is summarized in Table 2. The C content decreases from 97.9% to a minimum value of 82.7% after 10 min of plasma treatment, while the N and O contents both increases. The O increase in the treated sample can be attributed to the following reasons as we mentioned in Section "Plasma Parameters": Firstly, the chamber is not possible to achieve complete sealing and residual air inside cannot be fully eliminated. Even with 100%  $N_2$  introduced

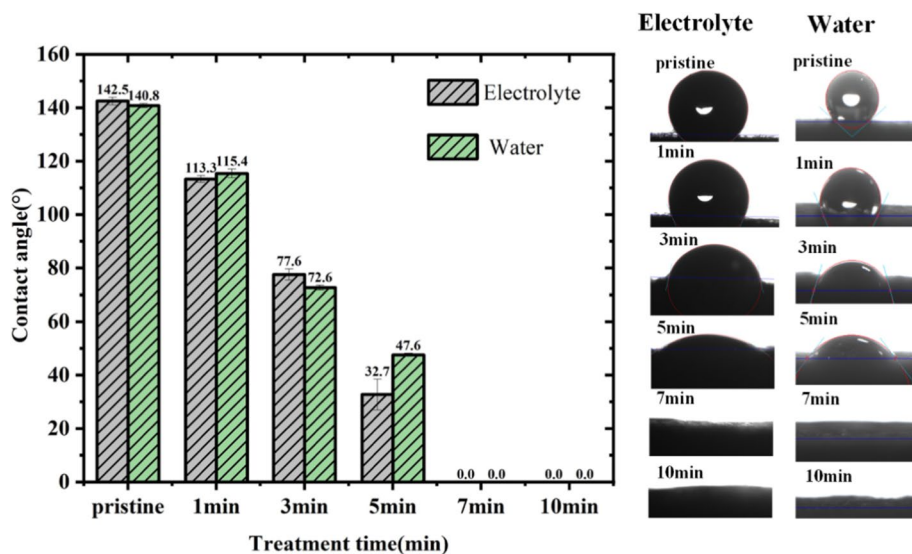
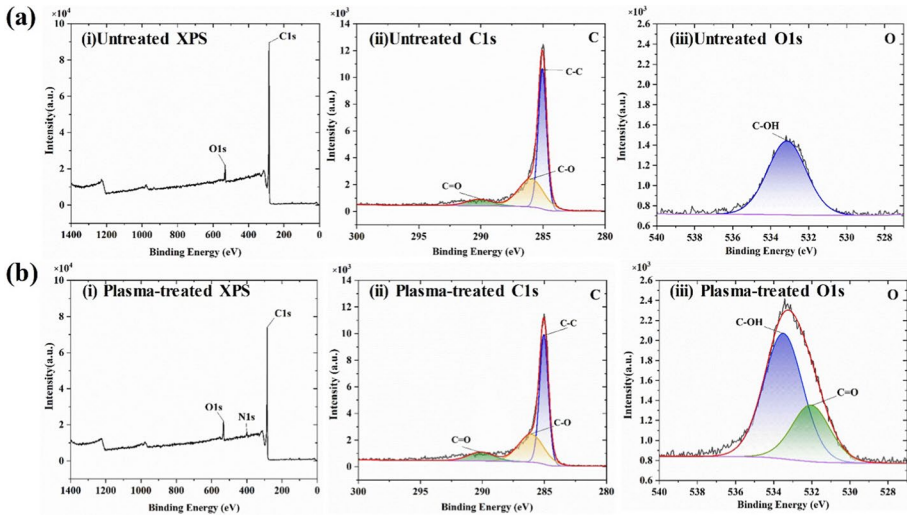


Fig. 8 Electrolyte and water contact angle of CF after  $N_2$  DBD treatment vs. treatment time





**Fig. 9** **a** XPS survey spectra of untreated CF of (i) full spectrum (ii) C1s and (iii) O1s. **b** XPS survey spectra of plasma-treated CF of (i) full spectrum (ii) C1s and (iii) O1s

**Table 2** Atomic content change on the CF surface vs. treatment time of N<sub>2</sub> DBD treatment

	Atomic content (%)			Atomic content ratio (%)	
	C	N	O	N/C	O/C
Pristine	97.9	0	2.3	0	2.3
1 min	91.9	0	8.1	0	8.8
3 min	87.2	1.2	11.6	1.4	13.3
5 min	86.5	1.5	12	1.7	13.8
7 min	85.4	2.8	11.8	3.3	13.8
10 min	82.7	3.6	13.6	4.4	16.4

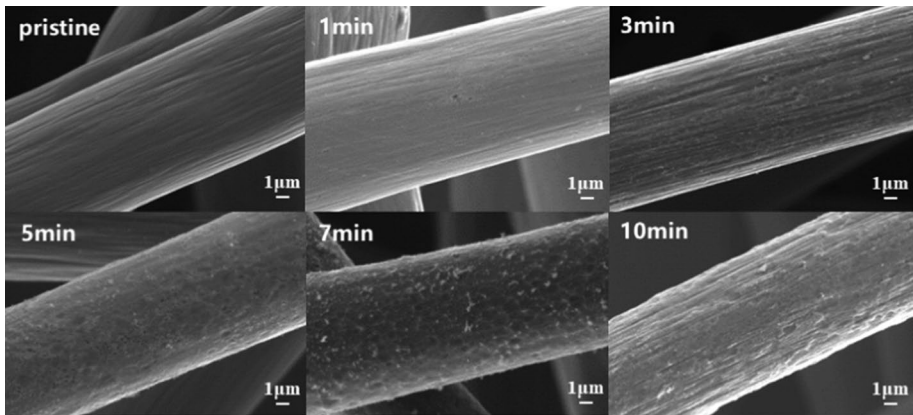
into the chamber, a small amount of O<sub>2</sub> may still be involved in the reaction. Secondly, plasma treatment can create structural defects [28], thus the unsaturated carbon atoms reacted with either oxygen attracted in the porous CF materials or the environmental oxygen to increase the O content. The detection of O element in the untreated CF also supported this hypothesis.

Table 3 presents the composition ratio of functional groups obtained from the curve fitting of C1s and O1s XPS spectrum. The C–C content decreases from 62.86% to 43.93% after 10 min treatment, and the C–OH content decreases from 100% to 45.63%. The oxygen-containing functional groups of C–O and C=O increases, which are known to be electrochemically active sites for vanadium redox reaction [13, 29]. In the O1s curve fitting, the functional groups were primarily C–OH before treatment, and the majority of which were oxidized into C=O after modification.

Furthermore, the surface morphology was observed by SEM, as shown in Fig. 10. The results show that plasma modification not only increases the nitrogen and oxygen content but also causes physical change on the carbon fibers, leading to an increase in

**Table 3** Chemical composition ratio of functional groups from curve fitting of C1s and O1s XPS spectra for various treatment time of N<sub>2</sub> plasma treatment

(%)	C1(C–C)	C2(C–O)	C3(C=O)
BE(eV)	285.0±0.02	285.9±0.1	289.9±0.1
Pristine	62.86	27.22	9.92
1 min	54.6	34.86	10.54
3 min	53.47	35.46	11.07
5 min	48.44	38.68	12.88
7 min	44.57	42.33	13.09
10 min	43.93	42.57	13.50
(%)	O1(C–OH)	O2(C=O)	
BE (eV)	533.3±0.1	531.7±0.05	
Pristine	100	–	
1 min	100	–	
3 min	81.01	18.99	
5 min	72.73	27.27	
7 min	56.91	43.09	
10 min	45.63	54.37	

**Fig. 10** Morphological change of the pristine and N<sub>2</sub> DBD-treated CFs by SEM with 5000 times magnification

surface roughness. The pristine fibers had a smooth and flat surface, while the surface of the modified fibers exhibit dents that were caused by the etching effect of the DBD treatment.

Therefore, the increased oxygen functional groups (such as C–O, C=O) cause the improvement of the CF hydrophilicity [24], changing it from hydrophobic to hydrophilic. The increased roughness and oxygen functional groups both increase the reaction area and provide more active sites for the vanadium redox reactions then enhance the VRFB efficiency.

## Conclusion

In this study, we further improved the VRFB efficiency by modification of the commercial CF electrode using atmospheric DBD. We optimized the modification conditions by altering the discharge gas composition and the treatment time, and found that the CE, VE and EE of the VRFB increased with the increase of N<sub>2</sub> ratio in the N<sub>2</sub>/O<sub>2</sub> mixture and the treatment time. The VE, CE and EE reached up to an improvement of 12.8%, 7% and 13.2% after 10 min of N<sub>2</sub> DBD treatment, respectively. The CF hydrophilicity was found to be closely relate to the VRFB efficiency, in which the decrease of the electrolyte and water contact angle corresponds to the increase of the VRFB efficiency. The increased surface roughness and the hydrophilic functional groups after DBD treatment can provide more active sites for the redox reaction and increase the reaction area for the electrode, which further improved the VRFB efficiency.

**Author Contributions** YL and JL mainly completed the experiments and data preparation; Prof. ZX instructed all the experiments and figures; YL and ZX prepared the original manuscript; Dr. MG, Prof. KW and Prof. KJ helped with data analysis and mechanism discussion. Prof. KJ also provided equipment for some experiments.

**Funding** The authors are grateful for financial support from Interdisciplinary Fund of the Wuhan National High Magnetic Field Center (No. WHMFC202101).

**Data Availability** All data generated or analyzed during this study are included in this paper.

## Declarations

**Conflict of interest** The authors declare no conflict of interest.

## References

1. González Z, Vizireanu S, Dinescu G, Blanco C, Santamaría R (2012) Carbon nanowalls thin films as nanostructured electrode materials in vanadium redox flow batteries. *Nano Energy* 1:833–839
2. Dixon D, Babu DJ, Langner J, Bruns M, Pfaffmann L, Bhaskar A, Schneider JJ, Scheiba F, Ehrenberg H (2016) Effect of oxygen plasma treatment on the electrochemical performance of the rayon and polyacrylonitrile based carbon felt for the vanadium redox flow battery application. *J Power Sources* 332:240–248
3. Skyllas-Kazacos M, Cao L, Kazacos M, Kausar N, Mousa A (2016) Vanadium electrolyte studies for the vanadium redox battery—A review. *ChemSusChem* 9:1521–43
4. Taş M, Elden G (2022) A comprehensive review of carbon-based and metal-based electrocatalysts in the vanadium redox flow battery. *Energy Stor* 4:1–22
5. Wang WH, Wang XD (2007) Investigation of Ir-modified carbon felt as the positive electrode of an all-vanadium redox flow battery. *Electrochim Acta* 52:6755–6762
6. Schweiss R, Meiser C, Goh FWT (2017) Steady-state measurements of vanadium redox-flow batteries to study particular influences of carbon felt properties. *ChemElectroChem* 4:1969–1974
7. Yue L, Li W, Sun F, Zhao L, Xing L (2010) Highly hydroxylated carbon fibres as electrode materials of all-vanadium redox flow battery. *Carbon N. Y.* 48:3079–90
8. Liu S, Zhang W, Huang K (2006) Study on the electrochemical properties of carbon felt modified by PB and oxalic acid VRB application. *Chin J Power Sour* 30:395
9. Kaur A, Il Jeong K, Su Kim S, Woo Lim J (2022) Optimization of thermal treatment of carbon felt electrode based on the mechanical properties for high-efficiency vanadium redox flow batteries. *Compos Struct* 290:115546

10. Kim KJ, Kim YJ, Kim JH, Park MS (2011) The effects of surface modification on carbon felt electrodes for use in vanadium redox flow batteries. *Mater Chem Phys* 131:547–553
11. Cho YI, Park SJ, Hwang HJ, Lee JG, Jeon YK, Chu YH, Shul YG (2015) Effects of microwave treatment on carbon electrode for vanadium redox flow battery. *ChemElectroChem* 2:872–6
12. Li W, Zhang Z, Tang Y, Bian H, Ng TW, Zhang W, Lee CS (2016) Graphene-nanowall-decorated carbon felt with excellent electrochemical activity toward  $\text{VO}_2^+/\text{VO}_2^+$  couple for all vanadium redox flow battery. *Adv Sci* 3:1–7
13. Huang Y, Deng Q, Wu X, Wang S (2017) N, O Co-doped carbon felt for high-performance all-vanadium redox flow battery. *Int J Hydr Energy* 42:7177–7185
14. Permatasari A, Shin JW, Lee W, An J, Kwon Y (2021) The effect of plasma treated carbon felt on the performance of aqueous quinone-based redox flow batteries. *Int J Energy Res* 45:17878–17887
15. Dixon D, Babu DJ, Bhaskar A, Bruns HM, Schneider JJ, Scheiba F, Ehrenberg H (2019) Tuning the performance of vanadium redox flow batteries by modifying the structural defects of the carbon felt electrode *Beilstein. J Nanotechnol* 10:1698–1706
16. Mude NN, Bukke RN, Saha JK, Avis C, Jin J (2019) Highly stable, solution-processed Ga-doped IZTO thin film transistor by  $\text{Ar}/\text{O}_2$  plasma treatment. *Adv Electron Mater* 5:1900768
17. Dou S, Tao L, Wang R, El Hankari S, Chen R, Wang S (2018) Plasma-assisted synthesis and surface modification of electrode materials for renewable energy. *Adv Mater* 30:1–24
18. Bai C, Ning F, Pan S, Wang H, Li Y, Shen M, Zhou X (2022) Plasma treated carbon paper electrode greatly improves the performance of iron-hydrogen battery for low-cost energy storage. *Chinese Chem Lett* 33:1095–1099
19. Sun S, Wu Y, Zhu J, Lu C, Sun Y, Wang Z, Chen J (2022) Stabilizing plasma-induced highly nitrogen-deficient g-C<sub>3</sub>N<sub>4</sub> by heteroatom-refilling for excellent lithium-ion battery anodes. *Chem Eng J* 427:131032
20. Chen X, Li Y, Li M, Xiong Z (2022) Sterilization mechanism of helium/helium–oxygen atmospheric-pressure pulsed dielectric barrier discharge on membrane surface. *Plasma Sci Technol* 24:124015
21. Yin M, Huang J, Yu J, Chen G, Qu S, Wang X, Li C (2018) The polypropylene membrane modified by an atmospheric pressure plasma jet as a separator for lithium-ion button battery. *Electrochim Acta* 260:489–497
22. Chen JZ, Liao WY, Hsieh WY, Hsu CC, Chen YS (2015) All-vanadium redox flow batteries with graphite felt electrodes treated by atmospheric pressure plasma jets. *J Power Sources* 274:894–898
23. Lin CH, Zhuang YD, Tsai DG, Wei HJ, Liu TY (2020) Performance enhancement of vanadium redox flow battery by treated carbon felt electrodes of polyacrylonitrile using atmospheric pressure plasma. *Polymers* 12(6):1372
24. Chen SY, Kuo YL, Wang YM, Hsu WM, Chien TH, Lin CF, Kuo CH, Okino A, Chiang TC (2021) Atmospheric pressure tornado plasma jet of polydopamine coating on graphite felt for improving electrochemical performance in vanadium redox flow batteries. *Catalysts* 11(5):627
25. Lu C, Chen X, Wang Y, Zhu Y, Zou Z, Xiong Z (2022) Effect of dielectric parameters on the transformation of operation mode and the energy cost of nitrogen fixation of surface microdischarge in air. *Plasma Process Polym* 19(2):2100107
26. Santak V, Zaplotnik R, Tarle Z, Milosevic S (2015) optical emission spectroscopy of an atmospheric pressure plasma jet during tooth bleaching gel treatment. *Appl Spectrosc* 69:1327–1333
27. Hidalgo H, Tristant P, Denoirjean A, Desmaison J (2001) Microwave plasma enhanced CVD of aluminum oxide films: Influence of the deposition parameter on the films characteristics. *J Phys IV* 11:723–730
28. Bellani S, Najafi L, Prato M, Oropesa-Nuñez R, Martín-García B, Gagliani L, Mantero E, Marasco L, Bianca G, Zappia MI, Demirci C, Olivotto S, Mariucci G, Pellegrini V, Schiavetti M, Bonaccorso F (2021) Graphene-based electrodes in a vanadium redox flow battery produced by rapid low-pressure combined gas plasma treatments. *Chem Mater* 33:4106–4121
29. Han P, Yue Y, Liu Z, Xu W, Zhang L, Xu H, Dong S, Cui G (2011) Graphene oxide nanosheets/multi-walled carbon nanotubes hybrid as an excellent electrocatalytic material towards  $\text{VO}_2^+/\text{VO}_2^+$  redox couples for vanadium redox flow batteries. *Energy Environ Sci* 4:4710–4717

**Publisher's Note** Springer Nature remains neutral with regard to jurisdictional claims in published maps and institutional affiliations.

Springer Nature or its licensor (e.g. a society or other partner) holds exclusive rights to this article under a publishing agreement with the author(s) or other rightsholder(s); author self-archiving of the accepted manuscript version of this article is solely governed by the terms of such publishing agreement and applicable law.